Multipolar ferroelectricity in the Mott regime

Pengwei Zhao [1,*] Jiahao Yang [1,*] and Gang v. Chen [1,2,†]
[1]*International Center for Quantum Materials, School of Physics, Peking University, Beijing 100871, China*
[2]*Collaborative Innovation Center of Quantum Matter, Beijing 100871, China*

(Received 3 January 2025; revised 4 June 2025; accepted 5 June 2025; published 17 June 2025)

Ferroelectricity has been one major focus in modern fundamental research and technological applications. We consider the physical origin of improper ferroelectricity in Mott insulating materials. Beyond the well-known Katsura-Nagaosa-Balatsky inverse Dzyaloshinskii-Moriya mechanism for noncollinearly ordered magnets, we point out the induction of electric polarizations in multipolar-ordered Mott insulators. Using the multiflavor representation for the multipolar magnetic moments, we can show the crossover or transition from the pure inverse Dzyaloshinskii-Moriya mechanism to the pure multipolar origin for the ferroelectricity and also incorporate the intermediate regime with the mixture of both origins. We expect our results to inspire a reexamination of ferroelectricity in the multipolar-ordered magnets.

DOI: 10.1103/pm3h-pz2p

I. INTRODUCTION

The origin of electric polarization in solid-state systems has been an enduring subject in modern condensed matter physics. Even for noninteracting band insulators, this question turns out to be quite fundamental. It has been realized that the electric polarization of band insulators in the quantum case is actually multivalued and thus is related to some kind of phase variables [1–5]. Progress was made until the introduction of the Berry phase effects of the Bloch states of the band electrons, and it was pointed out that the electric polarization is related to the integration of the Berry phase of the Bloch electrons over the Brillouin zone [6,7]. This result and understanding were revived in the era of (magnetic) topological insulators, when the quantized axion magnetoelectric response was discovered [8]. In the Mott insulating regime, the degrees of freedom are localized spins and orbitals instead of physical electrons. Based on the irrelevance of the electron bands, it seems that the relation to the electron Berry phase is not directly applicable to the Mott regime. The emergence of improper ferroelectricity with the magnetic degrees of freedom in Mott insulators has been an interesting subject for multiferroics, in which electric polarization is considered to be the outcome of magnetism [9–26]. It is expected that the magnetoelectric coupling in multiferroic materials can enable the electric control of magnetism and vice versa [27,28]. One well-known mechanism for the improper ferroelectricity in Mott insulators is the Katsura-Nagaosa-Balatsky inverse Dzyaloshinskii-Moriya mechanism, which was proposed by connecting the electric polarization to the spin current for noncollinearly ordered magnets [12,15]. Despite the success of this mechanism, the origin of the ferroelectricity in the Mott regime has still not been fully resolved. Within the limit of our understanding, we think there are at least two more important aspects of this problem, and we explain below.

The first aspect is the local moment structure in the Mott regime. Often, the local moment is not simply the magnetic dipole moment with a pure spin-S contribution and could involve high-rank magnetic moments, such as magnetic quadrupole and octupole moments [29]. In the original inverse Dzyaloshinskii-Moriya mechanism, only the magnetic dipole moment is considered [12]. It is thus natural to explore the relation between the electric polarization and high-rank magnetic multipoles. The second aspect is the charge fluctuations, especially since the ferroelectricity is related to the charge degrees of freedom. While the charge fluctuations are suppressed in the strong Mott regime, they are quite significant in the weak Mott regime [30–32]. Although the mechanisms for the ferroelectricity extend to the weak Mott regime, the strong charge fluctuations in the weak Mott regime could induce new mechanisms for ferroelectricity. Moreover, the physical spin in the weak Mott regime is not very far from the electron on the metallic side, and thus, one may expect the Berry phase physics to extend to the weak Mott regime when the system is in certain spin liquid phases. In this work, we focus on the first aspect and will return to the second aspect in a later work.

We work in the strong Mott regime with multipolar order. In particular, for the specific $J = 1$ case, the multipolar ferroelectricity is narrowed down to the quadrupolar ferroelectricity. Other cases such as the octupolar ferroelectricity have been considered in Ref. [29]. We then explore the relationship between the electric polarization and the local magnetic moment and single out the contribution from the quadrupole moment. This mechanism is beyond the well-known inverse Dzyaloshinskii-Moriya mechanism and is referred to as "multipolar ferroelectricity." In the actual formulation of our calculation for $J = 1$, we are able to obtain the contributions from both the dipole and quadrupole channels and can continuously switch from the pure inverse

*These authors contributed equally to this work.
†Contact author: chenxray@pku.edu.cn

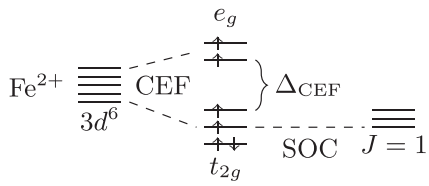

FIG. 1. Schematic diagram of the level splitting of the $3d$ orbitals of the Fe^{2+} ion in the octahedral environment. The crystal electric field (CEF) splits the fivefold $3d$ orbitals into the e_g and t_{2g} manifolds with an energy gap Δ_{CEF}. Arrows show the electron spin configuration on e_g and t_{2g} orbitals. Within the t_{2g} subspace, the spin-orbit coupling of $L = 1$ and $S = 2$ produces a new ground manifold with total angular momentum $J = 1$.

Dzyaloshinskii-Moriya mechanism to the pure quadrupolar ferroelectricity.

The remainder of this paper is organized as follows. Section II introduces the spin-orbit coupled states for the effective moment $J = 1$. An analysis of magnetic dipoles and quadruples carried by these states is also given in this section. In Sec. III, we consider a minimal three-site cluster model to illustrate the fundamental mechanism of multipolar ferroelectricity. After providing an analytical expression for electric polarization in Sec. IV, we summarize the paper with a discussion and conclusions in Sec. V.

II. SINGLE-ION PHYSICS

A. Ground states

The spin-orbit-entangled $J = 1$ local moment can arise from a magnetic ion, such as Fe^{2+}, which has a $3d^6$ electron configuration in an octahedral crystal field. In this environment, the crystal field splits the fivefold degenerate d orbitals into a t_{2g} triplet as the ground state and an e_g doublet, separated by an energy gap Δ_{CEF} [33,34]. Following Hund's first rule, we consider the high-spin configuration for $3d^6$, with $S = 2$ and an electron distribution of $t_{2g}^4 e_g^2$. As the t_{2g} shell is partially filled, threefold degeneracy exists for the orbital configuration, and the spin-orbit coupling (SOC) is active in the linear order. The total orbital angular momentum in this degenerate manifold is equivalent to an orbital moment $\boldsymbol{L}$ with $L = 1$. After the SOC $H_{SOC} = \lambda \boldsymbol{L} \cdot \boldsymbol{S}$ ($\lambda > 0$) is included, the total angular momentum $\boldsymbol{J} = \boldsymbol{L} + \boldsymbol{S}$ is used to label the local moment, and it has a threefold degenerate ground state manifold with $J = 1$ for the Fe^{2+} ion [35,36] (see Fig. 1).

In the following, the wave functions of the $J = 1$ moment are constructed explicitly, which is necessary for the later investigation of multipolar ferroelectricity. To begin with, we derive the effective orbital angular momentum $\boldsymbol{L}$ from the hole representation since six electrons are more than half filling. Thus, the orbital configuration of four holes is $t_{2g}^2 e_g^2$-like with three possibilities:

$$\begin{aligned} |a\rangle &= A^\dagger|0\rangle = d^\dagger_{3z^2} d^\dagger_{x^2-y^2} d^\dagger_{zx} d^\dagger_{xy} |0\rangle, \\ |b\rangle &= B^\dagger|0\rangle = d^\dagger_{3z^2} d^\dagger_{x^2-y^2} d^\dagger_{xy} d^\dagger_{yz} |0\rangle, \\ |c\rangle &= C^\dagger|0\rangle = d^\dagger_{3z^2} d^\dagger_{x^2-y^2} d^\dagger_{yz} d^\dagger_{zx} |0\rangle, \end{aligned} \tag{1}$$

where $|0\rangle$ is the vacuum state of the holes (full state of electrons); $d_a^\dagger$ creates a hole on the a orbital, with $a = 3z^2 - r^2, x^2 - y^2, xy, yz, zx$; and $3z^2$ refers to the $3z^2 - r^2$ orbital. Here we choose the quantization of $\boldsymbol{L}$ to be along the z direction. Based on the states in Eq. (1), we can construct the corresponding orbital angular momentum operators $\boldsymbol{L}$ and the eigenstates of L_z as

$$|L_z = \pm 1\rangle = \frac{1}{\sqrt{2}}[|a\rangle \pm i\,|b\rangle], \quad |L_z = 0\rangle = |c\rangle. \tag{2}$$

Regarding the spin-orbit coupling, the eigenstate of total angular momentum $|J, J_z\rangle$ is expressed in the decoupled representation of $|L, L_z, S, S_z\rangle$ through Clebsch-Gordan coefficients. This leads to threefold eigenstates with total angular momentum $J = 1$. The explicit forms in terms of individual holes are listed in Appendix B.

Regarding the SOC states $|J_z = \pm 1, 0\rangle$ as ground states of a single Fe^{2+} ion implies that the Jahn-Teller (JT) effect has been ignored. This approximation is justified for t_{2g} orbitals, which have a relatively weak JT effect. Concretely, the magnitude of JT distortions scales with the orbital-ligand overlap. In the octahedral environment, e_g orbitals (directed toward ligands) undergo strong distortion when they are unevenly occupied, whereas t_{2g} orbitals (oriented between ligands) display substantially weaker JT effects. Moreover, when SOC is dominant over the JT effect, the SOC splits the degenerate t_{2g} manifold into well-separated spin-orbit states described by spin-orbit entangled "pseudospins," and the lattice remains largely undistorted. The SOC not only can suppress the JT distortion but can also enable effectively larger spin-orbital pseudospins [37]. Therefore, we can safely neglect JT effects in our analysis up to the leading order. Notably, quantitative analysis of SOC versus JT competition reveals that JT effects are generally suppressed for typical SOC strengths in $4d$ and $5d$ ions [38].

B. Magnetic moments

To reveal the effect of the quadrupole moment, we construct a dipole-order-free basis in the $J = 1$ manifold as

$$\begin{aligned} |x\rangle &= \frac{1}{\sqrt{2}}(|J_z = -1\rangle - |J_z = +1\rangle), \\ |y\rangle &= \frac{i}{\sqrt{2}}(|J_z = -1\rangle + |J_z = +1\rangle), \\ |z\rangle &= |J_z = 0\rangle, \end{aligned} \tag{3}$$

with a general state in the $J = 1$ manifold expressed by

$$|\psi\rangle = b_x\,|x\rangle + b_y\,|y\rangle + b_z\,|z\rangle, \tag{4}$$

where the coefficient vector $\boldsymbol{b} = (b_x, b_y, b_z)$ is, in general, complex. Since the total angular momentum of $J = 1$ allows for the presence of high-rank magnetic moments, it can accommodate both the dipole and quadrupole moments. The dipole moment is directly related to the local moment $\boldsymbol{J}$ itself, while the quadrupole moment $Q_{\mu\nu}$ is given by the rank-2 tensor,

$$Q_{\mu\nu} = \frac{1}{2}\{J_\mu, J_\nu\} - \frac{\boldsymbol{J}^2}{3}\delta_{\mu\nu}, \quad \mu, \nu \in \{x, y, z\}, \tag{5}$$

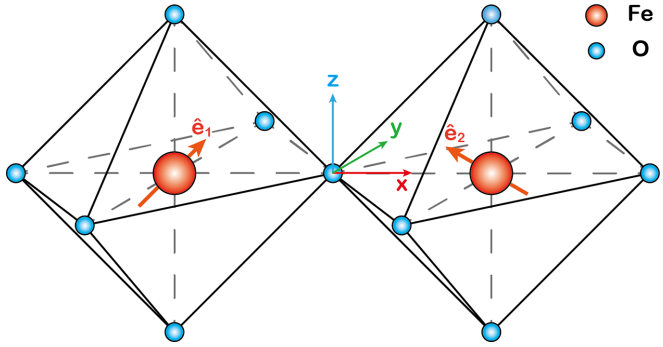

FIG. 2. The corner-sharing octahedral cluster. The red solid arrows at each Fe ion indicate the direction of noncollinear magnetic ordering $\hat{\boldsymbol{e}}$. The vector determines the "direction" of the quadrupolar order when the dipolar order is quenched.

where $\delta_{\mu\nu}$ is the Kronecker delta symbol. $Q_{\mu\nu}$ can be understood as the second-order Steven's operator, which reveals the underlying spin quadrupole orders in the system [39]. In the state $|\psi\rangle$, the dipole and quadrupole orders are evaluated as

$$\langle\psi|\boldsymbol{J}|\psi\rangle = -i\boldsymbol{b}^* \times \boldsymbol{b}, \tag{6}$$

and

$$\langle\psi|Q_{\mu\nu}|\psi\rangle = \tfrac{1}{3}\delta_{\mu\nu} - \tfrac{1}{2}(b_\mu^* b_\nu + b_\nu^* b_\mu), \tag{7}$$

indicating that their existence and disappearance can be controlled by tuning the vector $\boldsymbol{b}$. The symmetric tensor $Q_{\mu\nu}$ has five independent components, $Q_{3z^2-r^2}$, $Q_{x^2-y^2}$, Q_{xy}, Q_{yz}, and Q_{zx}. The presence of the quadrupole moments in the local Hilbert space suggests that these high-spin systems could exhibit richer ferroelectric behaviors beyond those explained by the inverse Dzyaloshinskii-Moriya mechanism. Moreover, when the dipole moment vanishes under the condition $\boldsymbol{b}^* \parallel \boldsymbol{b}$, the state $|\psi\rangle$ retains only the quadrupole order. This enables the exploration of the mechanism from which the ferroelectricity arises purely from the quadrupole orders.

To incorporate both the dipolar order and quadrupolar order for the Mott insulator, we treat these orders as a mean field coupled to the local spin $\boldsymbol{J}$ in the relevant channel. We consider a generic local coupling, $H_0 = J_1\hat{\boldsymbol{e}}\cdot\boldsymbol{J} + J_2(\hat{\boldsymbol{e}}\cdot\boldsymbol{J})^2$, where the magnetic ordering vector $\hat{\boldsymbol{e}} = (\sin\theta\cos\phi, \sin\theta\sin\phi, \cos\theta)$ for the $J = 1$ local momentum and the couplings $J_{1,2} > 0$. Under the application of H_0, the ground state of the d^6 electrons of the Fe^{2+} ion can be described as $|\psi\rangle$ with a $J_{1,2}$-dependent vector $\boldsymbol{b}$ (see Appendix C). In particular, when $J_1 < J_2$, the vector $\boldsymbol{b}$ is identical to the unit vector $\hat{\boldsymbol{e}}$, and a spin state without the magnetic dipole orders is established.

III. THREE-SITE CLUSTER

We consider a minimal model consisting of two corner-sharing octahedra (see Fig. 2). Without loss of generality, the cluster is oriented along the x direction, and the orbital quantization is along the z direction. Due to the finite intersite overlap between the $3d$ orbitals of the Fe sites and the $2p$ orbitals of the oxygen site, i.e., the π bonding from the t_{2g} orbitals and the σ bonding from the e_g orbital, the electron hopping is described by the following perturbative Hamiltonian:

$$H_{\rm hop} = \sum_{\sigma;\alpha=y,z} t(d^\dagger_{1,x\alpha,\sigma}p_{\alpha\sigma} - d^\dagger_{2,x\alpha,\sigma}p_{\alpha\sigma}) + \sum_\sigma t_0(d^\dagger_{1,3x^2,\sigma}p_{x\sigma} - d^\dagger_{2,3x^2,\sigma}p_{x\sigma}) + \text{H.c.}, \tag{8}$$

where t and t_0 are the hopping parameters, $d^\dagger_{i,a,\sigma}$ ($i = 1, 2$, $a = xy, xz, 3x^2 - r^2$, $\sigma = \uparrow, \downarrow$) creates a hole with spin σ in the d orbital of the ith Fe site, $p^\dagger_{\beta\sigma}$ ($\beta = x, y, z$) creates a hole with spin σ in the p orbital of O, and $3x^2$ refers to the $3x^2 - r^2$ orbital. The $3x^2$ orbital is related to the $3z^2$ and $x^2 - y^2$ orbitals by the relation $d^\dagger_{i,3x^2,\sigma} = \frac{\sqrt{3}}{2}d^\dagger_{i,x^2-y^2,\sigma} - \frac{1}{2}d^\dagger_{i,3z^2,\sigma}$. Therefore, the total Hamiltonian for the three-site cluster is

$$H = H_{\text{Fe},1} + H_{\text{Fe},2} + H_{\rm O} + H_{\rm hop}, \tag{9}$$

where the first three terms describe the on-site electron correlations leading to different ground states, such as $|\psi\rangle$ in Eq. (4) for the d^6 electrons at the Fe site.

We take the electron-doped Fe-based Mott insulator as an example, where the d^6 and d^7 electron configurations are considered for the two Fe sites and the net charge order is assumed to be absent. For the perturbation of the d^6 (d^7) configuration, we obtain an intermediate configuration of d^7 (d^8) due to the virtual hopping process. Furthermore, it should be noted that, owing to the strong on-site interaction and SOC, the electron configurations have to be reconstructed; the details are given in Appendix B.

In the hole representation, the ground state of the four holes (d^6) is given by $|\psi\rangle$ in Eq. (4). The low-energy physics of three holes (d^7) can be effectively described by a total angular momentum $J = 1/2$. We denote $|J_z = 1/2\rangle \equiv |\Uparrow\rangle$ and $|J_z = -1/2\rangle \equiv |\Downarrow\rangle$, and the ground state is $|\phi_i\rangle = a_{i\Uparrow}|\Uparrow\rangle + a_{i\Downarrow}|\Downarrow\rangle$, where $\boldsymbol{a}_i = (a_{i\Uparrow}, a_{i\Downarrow})$ is a normalized complex-valued vector. Hence, the ground state for the cluster is given by $|\Psi_0\rangle = \frac{1}{\sqrt{2}}(|\phi_1, \psi_2\rangle + |\psi_1, \phi_2\rangle)$. The notation $|\phi_1, \psi_2\rangle$ is shorthand notation for $\mathscr{P}|\phi_1\rangle \otimes |0\rangle \otimes |\psi_2\rangle$, where $\mathscr{P}$ is an operator ensuring fermionic antisymmetry. We have assumed the oxygen site is filled with electrons, i.e., lacks holes.

Due to $H_{\rm hop}$, an electron on the Fe site can hop to the oxygen site, or equivalently, a hole on the Fe site can hop to the oxygen site. With this hybridization process, the first-order perturbed (un-normalized) state is given by

$$\begin{aligned}|\Psi\rangle = {}& |\phi_1, \psi_2\rangle + |\psi_1, \phi_2\rangle \\ &+ \frac{1}{\Delta}\sum_{d^8,\alpha}|d_1^8, p_\alpha, \psi_2\rangle\langle d_1^8, p_\alpha, \psi_2|H_{\rm hop}|\phi_1, \psi_2\rangle \\ &+ \frac{1}{\Delta}\sum_{d^7,\alpha}|\phi_1, p_\alpha, d_2^7\rangle\langle\phi_1, p_\alpha, d_2^7|H_{\rm hop}|\phi_1, \psi_2\rangle \\ &+ \frac{1}{\Delta}\sum_{d^8,\alpha}|\psi_1, p_\alpha, d_2^8\rangle\langle\psi_1, p_\alpha, d_2^8|H_{\rm hop}|\psi_1, \phi_2\rangle \\ &+ \frac{1}{\Delta}\sum_{d^7,\alpha}|d_1^7, p_\alpha, \phi_2\rangle\langle d_1^7, p_\alpha, \phi_2|H_{\rm hop}|\psi_1, \phi_2\rangle,\end{aligned} \tag{10}$$

where the summation runs over all possible two-hole (d^8) and three-hole (d^7) states and all $2p$ orbitals of the oxygen.

The energy separation between a $2p$ orbital and d orbitals is approximated as Δ.

IV. ELECTRIC POLARIZATION

For the perturbed state $|\Psi\rangle$, the electric polarization $\boldsymbol{P} = \langle\Psi|e\boldsymbol{r}|\Psi\rangle$. The operator $\boldsymbol{r}$ is a many-body operator, which is a sum of the position vectors of all particles $\boldsymbol{r} = \sum_n \boldsymbol{r}_n$ if the first quantization language is used. After a detailed analysis, we find six nonvanishing contributions. The first four contributions are from

$$\begin{aligned}
&\langle\phi_1, \psi_2|\boldsymbol{r}|d_1^8, p_\alpha, \psi_2\rangle = \langle\phi_1|\boldsymbol{r}|d_1^8, p_\alpha\rangle,\\
&\langle\phi_1, \psi_2|\boldsymbol{r}|\phi_1, p_\alpha, d_2^7\rangle = \langle\psi_2|\boldsymbol{r}|p_\alpha, d_2^7\rangle,\\
&\langle\psi_1, \phi_2|\boldsymbol{r}|\psi_1, p_\alpha, d_2^8\rangle = \langle\phi_2|\boldsymbol{r}|p_\alpha, d_2^8\rangle,\\
&\langle\psi_1, \phi_2|\boldsymbol{r}|d_1^7, p_\alpha, \phi_2\rangle = \langle\psi_1|\boldsymbol{r}|d_1^7, p_\alpha\rangle,
\end{aligned} \tag{11}$$

each depending only on the single Fe site parameters. Hence, we refer to these as the on-site contributions to the electric polarization and denote them as $\boldsymbol{P}_{\rm on}$. The remaining terms, referred to as the intersite contributions and denoted as $\boldsymbol{P}_{\rm int}$, are given by

$$\begin{aligned}
&\langle\phi_1, \psi_2|\boldsymbol{r}|d_1^7, p_\alpha, \phi_2\rangle,\\
&\langle\psi_1, \phi_2|\boldsymbol{r}|\phi_1, p_\alpha, d_2^7\rangle,
\end{aligned} \tag{12}$$

which have a hybrid form involving $\boldsymbol{b}$ and $\boldsymbol{a}$. Other terms in $\langle\Psi|\boldsymbol{r}|\Psi\rangle$ vanish due to the orthogonality and the parity requirements.

The on-site contributions $\boldsymbol{P}_{\rm on}$ arise purely from the hybridization between the Fe ions and the ligand O ion. Since the on-site contributions are obtained for each Fe site, we can discuss their contribution separately, i.e., $\boldsymbol{P}_{\rm on} = \boldsymbol{P}_{1,\rm on} - \boldsymbol{P}_{2,\rm on}$. The on-site contribution from the hybridization between the ith Fe atom and the O atom can be obtained from the perturbative calculation

$$\begin{aligned}
\tilde{P}^x_{i,\rm on} = &\frac{49}{\sqrt{3}}\langle Q_{3z^2-r^2}\rangle_i + \langle Q_{x^2-y^2}\rangle_i - 3(\sqrt{3}-1)t_0 t^{-1}\\
&\times\left[2\langle Q_{xy}\rangle_i + \langle J_x\rangle_i^{(d^6)} + \langle J_y\rangle_i^{(d^6)}\right],
\end{aligned} \tag{13}$$

$$\tilde{P}^y_{i,\rm on} = -\langle Q_{xy}\rangle_i, \tag{14}$$

$$\tilde{P}^z_{i,\rm on} = \langle J_x\rangle_i^{(d^6)} - 8\langle J_x\rangle_i^{(d^7)}, \tag{15}$$

where we have introduced $\tilde{P}^\mu_{i,\rm on} = P^\mu_{i,\rm on}/s_\mu$, with $s_x = 4c$, $s_y = 2c$, $s_z = 10c$, and $c = etI/(480\Delta)$ accounting for the anisotropy. The integral I is the overlap between d orbitals and p orbitals and is given by

$$I = \int \mathrm{d}^3\boldsymbol{r}\, d_{xy}(\boldsymbol{r}) x p_y(\boldsymbol{r}) \tag{16}$$

and its cyclic permutations of x, y, and z. It is clear that both the quadrupole and dipole of the $J = 1$ states and the dipole of the $J = 1/2$ states make contributions to $\boldsymbol{P}_{\rm on}$. This result indicates that $\boldsymbol{P}_{\rm on}$ is finite as long as $\boldsymbol{P}_{1,\rm on} \neq \boldsymbol{P}_{2,\rm on}$, corresponding to the nonuniform alignment of the quadrupoles and dipole moments. The underlying origin is the fact that the finite $\boldsymbol{P}_{\rm on}$ arises from the inversion symmetry breaking of the local moments via the nonuniform ordering, instead of directly from an imbalanced charge density distribution. Thus, it belongs to the so-called improper ferroelectricity. Moreover, these on-site contributions to the electric polarization, which are absent in the case considered in the original work in Ref. [12], are essential in the many-electron configurations. Moreover, we can make a zeroth-order estimation to the order of magnitude for $P^{x,y,z}$. With the lattice constant $a = 5$ Å, $\boldsymbol{P} \sim c \sim 10^{-5}(t/\Delta)\ C/m^2$, which is consistent with the results for $Ga_{2-x}Fe_xO_3$ [40].

For the intersite contribution $\boldsymbol{P}_{\rm int}$, two Fe ions are hybridized. The full expressions for $\boldsymbol{P}_{\rm int}$ in terms of $\boldsymbol{a}_i$ and $\boldsymbol{b}_i$ ($i = 1, 2$) are given in Appendix D. Here, to explain the essence of the multipolar ferroelectricity, we simplify our discussion to two different cases: (1) d^7 states are uniform; (2) d^6 states are uniform.

In case 1, we set $\boldsymbol{a}_1 = \boldsymbol{a}_2 = (1, 0)$, such that the dipolar order of the d^7 states is collinear and along the z direction. The intersite contribution $\boldsymbol{P}_{\rm int}$ can be reduced as follows:

$$\tilde{P}^x_{\rm int} = 0, \tag{17}$$

$$\tilde{P}^y_{\rm int} = -[\hat{\boldsymbol{x}} \times (\boldsymbol{b}_1^* \times \boldsymbol{b}_2)]_y - 2ib^*_{1z}b_{2z} + \text{H.c.}, \tag{18}$$

$$\tilde{P}^z_{\rm int} = -[\hat{\boldsymbol{x}} \times (\boldsymbol{b}_1^* \times \boldsymbol{b}_2)]_z + i(b^*_{1y}b_{2z} + b^*_{1z}b_{2y}) + \text{H.c.} \tag{19}$$

The first terms in $\tilde{P}^y_{\rm int}$ and $\tilde{P}^y_{\rm int}$ resemble the inverse Dzyaloshinskii-Moriya mechanism [12], while the second terms endow the mechanism with some additional effects. For a generic $\boldsymbol{b}_1$ and $\boldsymbol{b}_2$, the dipolar and quadrupolar orders are concomitant. We single out the quadrupolar order by choosing $\boldsymbol{b}_1 = \hat{\boldsymbol{e}}_1$ and $\boldsymbol{b}_2 = \hat{\boldsymbol{e}}_2$ to be the real-valued unit vectors, in which the dipolar orders are quenched. We then establish the multipolar version of the inverse Dzyaloshinskii-Moriya mechanism,

$$\tilde{\boldsymbol{P}}_{\rm int} \sim \hat{\boldsymbol{x}} \times (\hat{\boldsymbol{e}}_1 \times \hat{\boldsymbol{e}}_2). \tag{20}$$

This indicates that in a system without noncollinear magnetic orders, finite electric polarization can still be generated from the nonuniform quadrupolar orders. This clearly goes beyond the scope of the original inverse Dzyaloshinskii-Moriya mechanism [12]. The difference is that our mechanism is now determined by the underlying vector $\hat{\boldsymbol{e}}$ of the quadrupole moment $Q_{\mu\nu}$ rather than the direction of the dipole moment.

In case 2, the d^6 states are taken to be uniform. We discuss how the quadrupolar orders and the dipolar orders of the d^6 states modify the inverse Dzyaloshinskii-Moriya mechanism of the d^7 states. Fixing $\boldsymbol{b}_1 = \boldsymbol{b}_2 = (0, 0, 1)$, we obtain $\tilde{P}^x_{\rm int} = \tilde{P}^z_{\rm int} = 0$ and

$$\tilde{P}^y_{\rm int} = -i(a^*_{1\Uparrow}a_{2\Uparrow} - a_{1\Uparrow}a^*_{2\Uparrow} - a^*_{1\Downarrow}a_{2\Downarrow} + a_{1\Downarrow}a^*_{2\Downarrow}). \tag{21}$$

Finite electric polarization is generated by the noncollinear order of the $J = 1/2$ dipole moments of the d^7 states. We find that

$$\tilde{P}^y_{\rm int} \sim \sin\theta_1 \sin\theta_2 \sin(\phi_1 - \phi_2), \tag{22}$$

with the two spinors of the d^7 states being $\boldsymbol{a}_1 = \frac{\alpha}{|\alpha|}e^{-i\phi}(\sin\frac{\theta_1}{2}, e^{i\phi_1}\cos\frac{\theta_1}{2})$ and $\boldsymbol{a}_2 = (\sin\frac{\theta_2}{2}, e^{i\phi_2}\cos\frac{\theta_2}{2})$, where $\phi = \phi_1 - \phi_2$ and $\alpha = e^{-i\phi/2}\cos\frac{\theta_1}{2}\cos\frac{\theta_2}{2} + e^{i\phi/2}\sin\frac{\theta_1}{2}\sin\frac{\theta_2}{2}$. This expression for $\tilde{P}^y_{\rm int}$ is consistent with the earlier results in Ref. [12]. It demonstrates the crossover from the multipolar

origin to the original inverse Dzyaloshinskii-Moriya mechanism for ferroelectricity.

V. DISCUSSION AND CONCLUSION

In this work, we considered a minimal cluster to demonstrate that quadrupolar-ordered magnets can make a pronounced contribution to ferroelectricity. The original inverse Dzyaloshinskii-Moriya mechanism revealed the presence of finite electric polarization under noncollinear magnetic dipolar orders. We generalized this formalism to cases with higher-rank magnetic moments. By tuning the quadrupolar order together with the dipolar order, we obtained a crossover or transition from the multipolar ferroelectricity to the dipolar ferroelectricity. Moreover, the coexistence of the quadrupolar and dipolar orders significantly modifies the inverse Dzyaloshinskii-Moriya mechanism. In general, we expect the multipolar ferroelectricity to occur widely in spin-orbit-coupled Mott insulators with large J moments. These insulators include $4d/5d$ materials [41–46], $4f/5f$ magnets [39,47,48], some $3d$ transition metal compounds [40,49], and hybrid orbital systems [50–52].

The interplay between the high-rank multipolar orders and the dipolar order can lead to rather rich behaviors at zero and finite temperatures. The quadrupolar order often does not break time reversal symmetry, while the dipolar order breaks time reversal symmetry. From the Ginzburg-Landau theory [43], the dipolar order can induce the quadrupolar order as a subsidiary order, but the reverse is not true. Moreover, the quadrupolar order can persist up to a higher temperature than the dipolar order [53,54]. In terms of the ferroelectricity, quadrupolar ferroelectricity can occur at a higher temperature than dipolar ferroelectricity. Quadrupolar ferroelectricity further enriches the magnetoelectric response. The previously proposed "double-leaf Riemann surface topological converse magnetoelectricity" for the dipolar ferroelectricity [55], which dictates the half-periodic response of the magnetic dipolar moment to the external electric field, could generalize to quadrupolar ferroelectricity. More interestingly, in the case when the quadrupolar order itself is induced by the dipolar order, such a double-leaf Riemann surface topological converse magnetoelectricity could be further complicated because the response of the dipolar order to the variation of the quadrupolar order is another level of the double-leaf Riemann surface. Likewise, the previously proposed topological Roman surface realized by dipolar-order-induced ferroelectric polarization [56] can be further complicated for quadrupolar ferroelectricity with intertwined structures of the dipolar and quadrupolar orders.

To summarize, our work indicates a multipolar origin for the ferroelectricity in Mott insulators, even in the absence of the dipolar order. It provides a framework that unifies dipolar- and multipolar-based electric polarization. This framework may provide a better understanding of unconventional ferroelectric materials and experimental guidance for the design of materials with tunable multiferroic properties.

ACKNOWLEDGMENTS

This work is supported by the Ministry of Science and Technology of the People's Republic of China under Grant No. 2021YFA1400300 and by the Fundamental Research Funds for the Central Universities, Peking University.

DATA AVAILABILITY

No data were created or analyzed in this study.

APPENDIX A: REVIEW OF ATOMIC ORBITALS

In this Appendix, we provide a brief review of atomic orbitals and introduce our notations. For those who are familiar with atomic orbitals, this Appendix can be skipped.

When we talk about atomic orbitals, we are talking about the eigenstates of hydrogen and hydrogenlike atoms. Basic quantum mechanics tells us that real space wave functions of atomic orbitals are given by $\psi_{n,l,m}(\boldsymbol{r}) = R_{n,l}(r)Y_{l,m}(\theta,\phi)$. The angular part $Y_{l,m}(\theta,\phi)$ is the complex-valued spherical harmonics, while the radial part $R_{n,l}(r)$ is real valued. Eigenstates in the form of $\psi_{n,l,m}(\boldsymbol{r})$ are called complex orbitals. In practice, people usually use real orbitals, which are linear combinations of complex orbitals. Following the Condon-Shortley phase convention, we define real orbitals as

$$\psi^{\text{real}}_{n,l,m}(\boldsymbol{r}) = \begin{cases} \sqrt{2}(-1)^m \text{Re}\psi_{n,l,|m|}(\boldsymbol{r}) = \frac{1}{\sqrt{2}}[\psi_{n,l,-|m|}(\boldsymbol{r}) + (-1)^m \psi_{n,l,|m|}(\boldsymbol{r})], & m > 0, \\ \psi_{n,l,|m|}(\boldsymbol{r}), & m = 0, \\ \sqrt{2}(-1)^m \text{Im}\psi_{n,l,|m|}(\boldsymbol{r}) = \frac{i}{\sqrt{2}}[\psi_{n,l,-|m|}(\boldsymbol{r}) - (-1)^m \psi_{n,l,|m|}(\boldsymbol{r})], & m < 0. \end{cases} \tag{A1}$$

These orbitals are purely real and usually labeled by harmonic polynomials. For example, p orbitals ($l = 1$) are given by

$$\begin{aligned} \psi_{n,x} &= \psi^{\text{real}}_{n,1,+1} = \frac{1}{\sqrt{2}}(\psi_{n,1,-1} - \psi_{n,1,+1}) = R_{n,1}\sqrt{\frac{3}{4\pi}}\frac{x}{r}, \\ \psi_{n,z} &= \psi^{\text{real}}_{n,1,0} = \psi_{n,1,0} = R_{n,1}\sqrt{\frac{3}{4\pi}}\frac{z}{r}, \\ \psi_{n,y} &= \psi^{\text{real}}_{n,1,-1} = \frac{i}{\sqrt{2}}(\psi_{n,l,-1} + \psi_{n,l,+1}) = R_{n,1}\sqrt{\frac{3}{4\pi}}\frac{y}{r}. \end{aligned} \tag{A2}$$

d orbitals ($l = 2$) are given by

$$\psi_{n,x^2-y^2} = \psi^{\text{real}}_{n,2,+2} = \frac{1}{\sqrt{2}}(\psi_{n,2,-2} + \psi_{n,2,+2}) = R_{n,2}\frac{1}{4}\sqrt{\frac{15}{\pi}}\frac{x^2-y^2}{r^2},$$

$$\psi_{n,zx} = \psi^{\text{real}}_{n,2,+1} = \frac{1}{\sqrt{2}}(\psi_{n,2,-1} - \psi_{n,2,+1}) = R_{n,2}\frac{1}{2}\sqrt{\frac{15}{\pi}}\frac{zx}{r^2},$$

$$\psi_{n,3z^2-r^2} = \psi^{\text{real}}_{n,2,0} = \psi_{n,2,0} = R_{n,2}\frac{1}{2}\sqrt{\frac{5}{\pi}}\frac{3z^2-r^2}{r^2},$$

$$\psi_{n,yz} = \psi^{\text{real}}_{n,2,-1} = \frac{i}{\sqrt{2}}(\psi_{n,2,-1} + \psi_{n,2,+1}) = R_{n,2}\frac{1}{2}\sqrt{\frac{15}{\pi}}\frac{yz}{r^2},$$

$$\psi_{n,xy} = \psi^{\text{real}}_{n,2,-2} = \frac{i}{\sqrt{2}}(\psi_{n,2,-2} - \psi_{n,2,+2}) = R_{n,2}\frac{1}{2}\sqrt{\frac{15}{\pi}}\frac{xy}{r^2}. \tag{A3}$$

APPENDIX B: MANY-BODY STATES FOR DIFFERENT ELECTRON CONFIGURATIONS

Throughout our paper, we are working with the $3d^n$ configurations of Fe atoms. In this environment of an octahedral crystal field, the crystal field splits the fivefold degenerate d orbitals into a t_{2g} triplet as the ground state and an e_g doublet, separated by an energy gap Δ_{cry}. We consider the situation in which Δ_{cry} is smaller than the on-site repulsion of each orbital. Then electrons tend to occupy different orbitals rather than fill t_{2g}. In this circumstance, we analyze the many-body states for d^6, d^7, and d^8 electron configurations.

1. $d^6 = t_{2g}^4 e_g^2$ configuration

For the d^6 electron configuration, there are two electrons in e_g orbitals and four electrons in t_{2g} orbitals. Thus, we can denote d^6 as $t_{2g}^4 e_g^2$. There are three possibilities to arrange the four electrons in t_{2g} orbitals, giving rise to threefold orbital states. Since six electrons are more than half filling, it is more convenient to use the hole representation. In the hole representation, threefold orbital states are given by

$$\begin{aligned}
|a\rangle &= A^\dagger|0\rangle = d^\dagger_{3z^2-r^2} d^\dagger_{x^2-y^2} d^\dagger_{zx} d^\dagger_{xy}\,|0\rangle,\\
|b\rangle &= B^\dagger|0\rangle = d^\dagger_{3z^2-r^2} d^\dagger_{x^2-y^2} d^\dagger_{xy} d^\dagger_{yz}\,|0\rangle,\\
|c\rangle &= C^\dagger|0\rangle = d^\dagger_{3z^2-r^2} d^\dagger_{x^2-y^2} d^\dagger_{yz} d^\dagger_{zx}\,|0\rangle,
\end{aligned} \tag{B1}$$

where $d^\dagger_\alpha$ creates a hole at the orbital α with arbitrary spin and $|0\rangle$ is the vacuum state of the holes. The projection of the physical orbital angular momentum $\boldsymbol{L}_{\text{physical}}$ onto the threefold orbital states gives an effective angular momentum $\boldsymbol{L} \cong -\boldsymbol{L}_{\text{physical}}$ with a quantum number $L = 1$. The eigenstates of L_z are

$$\begin{aligned}
|L_z = +1\rangle &= \frac{1}{\sqrt{2}}(|a\rangle + i\,|b\rangle),\\
|L_z = 0\rangle &= |c\rangle,\\
|L_z = -1\rangle &= \frac{1}{\sqrt{2}}(|a\rangle - i\,|b\rangle).
\end{aligned} \tag{B2}$$

Hund's first rule tells us the d^6 configuration has a total spin $\boldsymbol{S}$ with spin quantum number $S = 2$. The eigenstates of S_z are given by

$$\begin{aligned}
|S_z = 2\rangle &= |\uparrow\uparrow\uparrow\uparrow\rangle,\\
|S_z = 1\rangle &= \frac{1}{2}(|\uparrow\uparrow\uparrow\downarrow\rangle + |\uparrow\uparrow\downarrow\uparrow\rangle + |\uparrow\downarrow\uparrow\uparrow\rangle + |\downarrow\uparrow\uparrow\uparrow\rangle),\\
|S_z = 0\rangle &= \frac{1}{\sqrt{6}}(|\uparrow\uparrow\downarrow\downarrow\rangle + |\uparrow\downarrow\uparrow\downarrow\rangle + |\uparrow\downarrow\downarrow\uparrow\rangle + |\downarrow\uparrow\uparrow\downarrow\rangle + |\downarrow\uparrow\downarrow\uparrow\rangle + |\downarrow\downarrow\uparrow\uparrow\rangle),\\
|S_z = -1\rangle &= \frac{1}{2}(|\downarrow\uparrow\uparrow\uparrow\rangle + |\uparrow\downarrow\uparrow\uparrow\rangle + |\uparrow\uparrow\downarrow\uparrow\rangle + |\uparrow\uparrow\uparrow\downarrow\rangle),\\
|S_z = -2\rangle &= |\downarrow\downarrow\downarrow\downarrow\rangle.
\end{aligned} \tag{B3}$$

Then, we consider the spin-orbital coupling (SOC) $H_{\text{SOC}} = \lambda \boldsymbol{L}\cdot\boldsymbol{S}$ with the coupling constant $\lambda > 0$. We can define the total angular momentum $\boldsymbol{J} = \boldsymbol{L} + \boldsymbol{S}$ and write $H_{\text{SOC}} = \lambda(\boldsymbol{J}^2 - \boldsymbol{L}^2 - \boldsymbol{S}^2)/2$. Thus, the SOC ground states are given by the quantum

number $J = 1$. Utilizing the Clebsch-Gordan coefficients, we obtain

$$\begin{aligned}
|J_z = 1\rangle &= \sqrt{\frac{1}{10}}\,|L_z = 1, S_z = 0\rangle - \sqrt{\frac{3}{10}}\,|L_z = 0, S_z = 1\rangle + \sqrt{\frac{3}{5}}\,|L_z = -1, S_z = 2\rangle,\\
|J_z = 0\rangle &= \sqrt{\frac{3}{10}}\,|L_z = 1, S_z = -1\rangle - \sqrt{\frac{2}{5}}\,|L_z = 0, S_z = 0\rangle + \sqrt{\frac{3}{10}}\,|L_z = -1, S_z = 1\rangle,\\
|J_z = -1\rangle &= \sqrt{\frac{3}{5}}\,|L_z = 1, S_z = -2\rangle - \sqrt{\frac{3}{10}}\,|L_z = 0, S_z = -1\rangle + \sqrt{\frac{1}{10}}\,|L_z = -1, S_z = 0\rangle.
\end{aligned} \tag{B4}$$

We also define three real-valued states from the threefold $J = 1$ states,

$$\begin{aligned}
|x\rangle &= X^\dagger\,|0\rangle = \frac{1}{\sqrt{2}}(|J_z = -1\rangle - |J_z = +1\rangle),\\
|y\rangle &= Y^\dagger\,|0\rangle = \frac{i}{\sqrt{2}}(|J_z = -1\rangle + |J_z = +1\rangle),\\
|z\rangle &= Z^\dagger\,|0\rangle = |J_z = 0\rangle.
\end{aligned} \tag{B5}$$

Combining Eqs. (B1) to (B3), we can express the states in Eq. (B5) in terms of the creation operators of a hole,

$$\begin{aligned}
\hat{X} = &\frac{1}{4\sqrt{15}}d^\dagger_{z^2,\uparrow}d^\dagger_{x^2-y^2,\uparrow}(-3d^\dagger_{yz,\uparrow}d^\dagger_{zx,\downarrow} - 3d^\dagger_{yz,\downarrow}d^\dagger_{zx,\uparrow} + 2id^\dagger_{xy,\downarrow}d^\dagger_{yz,\downarrow} - 6id^\dagger_{xy,\uparrow}d^\dagger_{yz,\uparrow} + 6d^\dagger_{zx,\uparrow}d^\dagger_{xy,\uparrow})\\
&+ \frac{1}{4\sqrt{15}}d^\dagger_{z^2,\downarrow}d^\dagger_{x^2-y^2,\downarrow}(3d^\dagger_{yz,\uparrow}d^\dagger_{zx,\downarrow} + 3d^\dagger_{yz,\downarrow}d^\dagger_{zx,\uparrow} - 6id^\dagger_{xy,\downarrow}d^\dagger_{yz,\downarrow} - 6d^\dagger_{zx,\downarrow}d^\dagger_{xy,\downarrow} + 2id^\dagger_{xy,\uparrow}d^\dagger_{yz,\uparrow})\\
&+ \frac{1}{4\sqrt{15}}d^\dagger_{z^2,\uparrow}d^\dagger_{x^2-y^2,\downarrow}(2id^\dagger_{xy,\uparrow}d^\dagger_{yz,\downarrow} + 2id^\dagger_{xy,\downarrow}d^\dagger_{yz,\uparrow} + 3d^\dagger_{yz,\downarrow}d^\dagger_{zx,\downarrow} - 3d^\dagger_{yz,\uparrow}d^\dagger_{zx,\uparrow})\\
&+ \frac{1}{4\sqrt{15}}d^\dagger_{z^2,\downarrow}d^\dagger_{x^2-y^2,\uparrow}(2id^\dagger_{xy,\uparrow}d^\dagger_{yz,\downarrow} + 2id^\dagger_{xy,\downarrow}d^\dagger_{yz,\uparrow} + 3d^\dagger_{yz,\downarrow}d^\dagger_{zx,\downarrow} - 3d^\dagger_{yz,\uparrow}d^\dagger_{zx,\uparrow}),
\end{aligned} \tag{B6}$$

$$\begin{aligned}
\hat{Y} = &-\frac{1}{4\sqrt{15}}id^\dagger_{z^2,\uparrow}d^\dagger_{x^2-y^2,\uparrow}(3d^\dagger_{yz,\uparrow}d^\dagger_{zx,\downarrow} + 3d^\dagger_{yz,\downarrow}d^\dagger_{zx,\uparrow} - 2d^\dagger_{zx,\downarrow}d^\dagger_{xy,\downarrow} + 6id^\dagger_{xy,\uparrow}d^\dagger_{yz,\uparrow} - 6d^\dagger_{zx,\uparrow}d^\dagger_{xy,\uparrow})\\
&+ \frac{1}{4\sqrt{15}}d^\dagger_{z^2,\downarrow}d^\dagger_{x^2-y^2,\downarrow}[-6d^\dagger_{xy,\downarrow}d^\dagger_{yz,\downarrow} - i(3d^\dagger_{yz,\uparrow}d^\dagger_{zx,\downarrow} + 3d^\dagger_{yz,\downarrow}d^\dagger_{zx,\uparrow} - 6d^\dagger_{zx,\downarrow}d^\dagger_{xy,\downarrow} - 2d^\dagger_{zx,\uparrow}d^\dagger_{xy,\uparrow})]\\
&- \frac{1}{4\sqrt{15}}id^\dagger_{z^2,\uparrow}d^\dagger_{x^2-y^2,\downarrow}(-2d^\dagger_{zx,\uparrow}d^\dagger_{xy,\downarrow} - 2d^\dagger_{zx,\downarrow}d^\dagger_{xy,\uparrow} + 3d^\dagger_{yz,\downarrow}d^\dagger_{zx,\downarrow} + 3d^\dagger_{yz,\uparrow}d^\dagger_{zx,\uparrow})\\
&- \frac{1}{4\sqrt{15}}id^\dagger_{z^2,\downarrow}d^\dagger_{x^2-y^2,\uparrow}(-2d^\dagger_{zx,\uparrow}d^\dagger_{xy,\downarrow} - 2d^\dagger_{zx,\downarrow}d^\dagger_{xy,\uparrow} + 3d^\dagger_{yz,\downarrow}d^\dagger_{zx,\downarrow} + 3d^\dagger_{yz,\uparrow}d^\dagger_{zx,\uparrow}),
\end{aligned} \tag{B7}$$

$$\begin{aligned}
\hat{Z} = &\frac{1}{4\sqrt{15}}d^\dagger_{z^2,\uparrow}d^\dagger_{x^2-y^2,\uparrow}(3d^\dagger_{zx,\uparrow}d^\dagger_{xy,\downarrow} + 3d^\dagger_{zx,\downarrow}d^\dagger_{xy,\uparrow} - 3id^\dagger_{xy,\uparrow}d^\dagger_{yz,\downarrow} - 3id^\dagger_{xy,\downarrow}d^\dagger_{yz,\uparrow} - 4d^\dagger_{yz,\downarrow}d^\dagger_{zx,\downarrow})\\
&+ \frac{1}{4\sqrt{15}}d^\dagger_{z^2,\uparrow}d^\dagger_{x^2-y^2,\downarrow}(3d^\dagger_{zx,\downarrow}d^\dagger_{xy,\downarrow} + 3d^\dagger_{zx,\uparrow}d^\dagger_{xy,\uparrow} + 3id^\dagger_{xy,\downarrow}d^\dagger_{yz,\downarrow} - 3id^\dagger_{xy,\uparrow}d^\dagger_{yz,\uparrow} - 4d^\dagger_{yz,\uparrow}d^\dagger_{zx,\downarrow} - 4d^\dagger_{yz,\downarrow}d^\dagger_{zx,\uparrow})\\
&+ \frac{1}{4\sqrt{15}}d^\dagger_{z^2,\downarrow}d^\dagger_{x^2-y^2,\uparrow}(3d^\dagger_{zx,\downarrow}d^\dagger_{xy,\downarrow} + 3d^\dagger_{zx,\uparrow}d^\dagger_{xy,\uparrow} + 3id^\dagger_{xy,\downarrow}d^\dagger_{yz,\downarrow} - 3id^\dagger_{xy,\uparrow}d^\dagger_{yz,\uparrow} - 4d^\dagger_{yz,\uparrow}d^\dagger_{zx,\downarrow} - 4d^\dagger_{yz,\downarrow}d^\dagger_{zx,\uparrow})\\
&+ \frac{1}{4\sqrt{15}}d^\dagger_{z^2,\downarrow}d^\dagger_{x^2-y^2,\downarrow}(3d^\dagger_{zx,\uparrow}d^\dagger_{xy,\downarrow} + 3d^\dagger_{zx,\downarrow}d^\dagger_{xy,\uparrow} + 3id^\dagger_{xy,\uparrow}d^\dagger_{yz,\downarrow} + 3id^\dagger_{xy,\downarrow}d^\dagger_{yz,\uparrow} - 4d^\dagger_{yz,\uparrow}d^\dagger_{zx,\uparrow}).
\end{aligned} \tag{B8}$$

A generic state in the threefold $J = 1$ space can be expressed as

$$|\psi\rangle = b_x\,|x\rangle + b_y\,|y\rangle + b_z\,|z\rangle, \tag{B9}$$

where $\boldsymbol{b} = (b_x, b_y, b_z)$ is a complex-valued vector that satisfies the normalization $\boldsymbol{b}^* \cdot \boldsymbol{b} = 1$.

2. $d^7 = t_{2g}^5 e_g^2$ configuration

For the d^7 electron configuration, there are two electrons in the e_g orbitals and five electrons in the t_{2g} orbitals. Thus, we can denote d^7 as $t_{2g}^5 e_g^2$. There are three possibilities to arrange the five electrons in the t_{2g} orbitals, giving rise to threefold orbital

states. In the hole representation, threefold orbital states are given by

$$\begin{aligned}|d\rangle &= D^\dagger|0\rangle = d^\dagger_{3z^2-r^2}d^\dagger_{x^2-y^2}d^\dagger_{xy}\,|0\rangle,\\ |e\rangle &= E^\dagger|0\rangle = d^\dagger_{3z^2-r^2}d^\dagger_{x^2-y^2}d^\dagger_{yz}\,|0\rangle,\\ |f\rangle &= F^\dagger|0\rangle = d^\dagger_{3z^2-r^2}d^\dagger_{x^2-y^2}d^\dagger_{zx}\,|0\rangle.\end{aligned} \tag{B10}$$

The projection of the physical orbital angular momentum $\boldsymbol{L}_{\text{physical}}$ on the threefold orbital states gives an effective angular momentum $\boldsymbol{L} \cong -\boldsymbol{L}_{\text{physical}}$ with a quantum number $L = 1$. The eigenstates of L_z are

$$\begin{aligned}|L_z = +1\rangle &= \frac{1}{\sqrt{2}}(|e\rangle + i\,|f\rangle),\\ |L_z = 0\rangle &= |d\rangle,\\ |L_z = -1\rangle &= \frac{1}{\sqrt{2}}(|e\rangle - i\,|f\rangle).\end{aligned} \tag{B11}$$

Hund's first rule tells us the d^7 configuration has a total spin $\boldsymbol{S}$ with spin quantum number $S = 3/2$. The eigenstates of S_z are given by

$$\begin{aligned}|S_z = 3/2\rangle &= |\uparrow\uparrow\uparrow\rangle,\\ |S_z = 1/2\rangle &= \frac{1}{\sqrt{3}}(|\uparrow\uparrow\downarrow\rangle + |\uparrow\uparrow\downarrow\rangle + |\downarrow\uparrow\uparrow\rangle),\\ |S_z = -1/2\rangle &= \frac{1}{\sqrt{3}}(|\downarrow\downarrow\uparrow\rangle + |\downarrow\uparrow\downarrow\rangle + |\uparrow\downarrow\downarrow\rangle),\\ |S_z = -3/2\rangle &= |\downarrow\downarrow\downarrow\rangle.\end{aligned} \tag{B12}$$

After the SOC, the total angular momentum $\boldsymbol{J}$ of the ground states has a quantum number $J = 1/2$. These states are given by

$$\begin{aligned}|J_z = 1/2\rangle &= \phi^\dagger_{1/2}\,|0\rangle = \sqrt{\frac{1}{6}}\,|L_z = 1, S_z = -1/2\rangle - \sqrt{\frac{1}{3}}\,|L_z = 0, S_z = 1/2\rangle + \sqrt{\frac{1}{2}}\,|L_z = -1, S_z = 3/2\rangle,\\ |J_z = -1/2\rangle &= \phi^\dagger_{-1/2}\,|0\rangle = \sqrt{\frac{1}{2}}\,|L_z = 1, S_z = -3/2\rangle - \sqrt{\frac{1}{3}}\,|L_z = 0, S_z = -1/2\rangle + \sqrt{\frac{1}{6}}\,|L_z = -1, S_z = 1/2\rangle.\end{aligned} \tag{B13}$$

Using Eqs. (B11) and (B12), we can write Eq. (B13) in terms of hole operators,

$$\begin{aligned}\phi^\dagger_{1/2} = &-\tfrac{1}{3}d^\dagger_{z^2,\uparrow}d^\dagger_{x^2-y^2,\downarrow}d^\dagger_{xy,\downarrow} - \tfrac{1}{3}d^\dagger_{z^2,\downarrow}d^\dagger_{x^2-y^2,\uparrow}d^\dagger_{xy,\downarrow} - \tfrac{1}{3}d^\dagger_{z^2,\downarrow}d^\dagger_{x^2-y^2,\downarrow}d^\dagger_{xy,\uparrow} + \tfrac{1}{6}d^\dagger_{z^2,\uparrow}d^\dagger_{x^2-y^2,\uparrow}d^\dagger_{yz,\downarrow}\\ &+ \tfrac{1}{6}d^\dagger_{z^2,\uparrow}d^\dagger_{x^2-y^2,\downarrow}d^\dagger_{yz,\uparrow} + \tfrac{1}{6}d^\dagger_{z^2,\downarrow}d^\dagger_{x^2-y^2,\uparrow}d^\dagger_{yz,\uparrow} + \tfrac{1}{6}id^\dagger_{z^2,\uparrow}d^\dagger_{x^2-y^2,\uparrow}d^\dagger_{zx,\downarrow} + \tfrac{1}{6}id^\dagger_{z^2,\uparrow}d^\dagger_{x^2-y^2,\downarrow}d^\dagger_{zx,\uparrow}\\ &+ \tfrac{1}{6}id^\dagger_{z^2,\downarrow}d^\dagger_{x^2-y^2,\uparrow}d^\dagger_{zx,\uparrow} + \tfrac{1}{2}d^\dagger_{z^2,\downarrow}d^\dagger_{x^2-y^2,\downarrow}d^\dagger_{yz,\downarrow} - \tfrac{1}{2}id^\dagger_{z^2,\downarrow}d^\dagger_{x^2-y^2,\downarrow}d^\dagger_{zx,\downarrow},\end{aligned} \tag{B14}$$

$$\begin{aligned}\phi^\dagger_{-1/2} = &-\tfrac{1}{3}d^\dagger_{z^2,\uparrow}d^\dagger_{x^2-y^2,\downarrow}d^\dagger_{xy,\downarrow} - \tfrac{1}{3}d^\dagger_{z^2,\downarrow}d^\dagger_{x^2-y^2,\uparrow}d^\dagger_{xy,\downarrow} - \tfrac{1}{3}d^\dagger_{z^2,\downarrow}d^\dagger_{x^2-y^2,\downarrow}d^\dagger_{xy,\uparrow} + \tfrac{1}{6}d^\dagger_{z^2,\uparrow}d^\dagger_{x^2-y^2,\uparrow}d^\dagger_{yz,\downarrow}\\ &+ \tfrac{1}{6}d^\dagger_{z^2,\uparrow}d^\dagger_{x^2-y^2,\downarrow}d^\dagger_{yz,\uparrow} + \tfrac{1}{6}d^\dagger_{z^2,\downarrow}d^\dagger_{x^2-y^2,\uparrow}d^\dagger_{yz,\uparrow} + \tfrac{1}{6}id^\dagger_{z^2,\uparrow}d^\dagger_{x^2-y^2,\uparrow}d^\dagger_{zx,\downarrow} + \tfrac{1}{6}id^\dagger_{z^2,\uparrow}d^\dagger_{x^2-y^2,\downarrow}d^\dagger_{zx,\uparrow}\\ &+ \tfrac{1}{6}id^\dagger_{z^2,\downarrow}d^\dagger_{x^2-y^2,\uparrow}d^\dagger_{zx,\uparrow} + \tfrac{1}{2}d^\dagger_{z^2,\downarrow}d^\dagger_{x^2-y^2,\downarrow}d^\dagger_{yz,\downarrow} - \tfrac{1}{2}id^\dagger_{z^2,\downarrow}d^\dagger_{x^2-y^2,\downarrow}d^\dagger_{zx,\downarrow}.\end{aligned} \tag{B15}$$

3. $d^7 = t_{2g}^4 e_g^3$ configuration

After hopping, we have the d^7 electron configuration as intermediate states, with three electrons in the e_g orbitals and four electrons in the t_{2g} orbitals. Thus, we can denote d^7 as $t_{2g}^4 e_g^3$. There are three possibilities to arrange the four electrons in the t_{2g} orbitals, giving rise to threefold orbital states. There are two possibilities for the three electrons in the e_g orbitals. In the hole representation, threefold orbital states are also given by

$$\begin{aligned}|g\rangle &= G^\dagger|0\rangle = d^\dagger_{e_g}d^\dagger_{zx}d^\dagger_{xy}\,|0\rangle,\\ |h\rangle &= H^\dagger|0\rangle = d^\dagger_{e_g}d^\dagger_{xy}d^\dagger_{yz}\,|0\rangle,\\ |j\rangle &= J^\dagger|0\rangle = d^\dagger_{e_g}d^\dagger_{yz}d^\dagger_{zx}\,|0\rangle,\end{aligned} \tag{B16}$$

where e_g represents one of the e_g orbitals, either $3z^2 - r^2$ or $x^2 - y^2$. The projection of the physical orbital angular momentum $\boldsymbol{L}_{\text{physical}}$ on the threefold orbital states gives an effective angular momentum $\boldsymbol{L} \cong -\boldsymbol{L}_{\text{physical}}$ with a quantum number $L = 1$. The

eigenstates of L_z are similar to Eqs. (B11). Hund's first rule tells us the d^7 configuration has a total spin $\boldsymbol{S}$ with spin quantum number $S = 3/2$. The eigenstates of S_z are similar to Eqs. (B12). After the SOC, the total angular momentum $\boldsymbol{J}$ of the ground states has quantum number $J = 1/2$. These states are similar to Eqs. (B13). Therefore, we can obtain the ground state in terms of hole operators,

$$\begin{aligned}\phi^\dagger_{1/2} = &-\tfrac{1}{3}d^\dagger_{e_g,\uparrow}d^\dagger_{zx,\downarrow}d^\dagger_{xy,\downarrow} - \tfrac{1}{3}d^\dagger_{e_g,\downarrow}d^\dagger_{zx,\uparrow}d^\dagger_{xy,\downarrow} - \tfrac{1}{3}d^\dagger_{e_g,\downarrow}d^\dagger_{zx,\downarrow}d^\dagger_{xy,\uparrow} + \tfrac{1}{6}d^\dagger_{e_g,\uparrow}d^\dagger_{xy,\uparrow}d^\dagger_{yz,\downarrow}\\ &+ \tfrac{1}{6}d^\dagger_{e_g,\uparrow}d^\dagger_{xy,\downarrow}d^\dagger_{yz,\uparrow} + \tfrac{1}{6}d^\dagger_{e_g,\downarrow}d^\dagger_{xy,\uparrow}d^\dagger_{yz,\uparrow} + \tfrac{1}{6}id^\dagger_{e_g,\uparrow}d^\dagger_{yz,\uparrow}d^\dagger_{zx,\downarrow} + \tfrac{1}{6}id^\dagger_{e_g,\uparrow}d^\dagger_{yz,\downarrow}d^\dagger_{zx,\uparrow}\\ &+ \tfrac{1}{6}id^\dagger_{e_g,\downarrow}d^\dagger_{yz,\uparrow}d^\dagger_{zx,\uparrow} + \tfrac{1}{2}d^\dagger_{e_g,\downarrow}d^\dagger_{xy,\downarrow}d^\dagger_{yz,\downarrow} - \tfrac{1}{2}id^\dagger_{e_g,\downarrow}d^\dagger_{yz,\downarrow}d^\dagger_{zx,\downarrow},\end{aligned} \tag{B17}$$

$$\begin{aligned}\phi^\dagger_{-1/2} = &-\tfrac{1}{3}d^\dagger_{e_g,\uparrow}d^\dagger_{zx,\downarrow}d^\dagger_{xy,\downarrow} - \tfrac{1}{3}d^\dagger_{e_g,\downarrow}d^\dagger_{zx,\uparrow}d^\dagger_{xy,\downarrow} - \tfrac{1}{3}d^\dagger_{e_g,\downarrow}d^\dagger_{zx,\downarrow}d^\dagger_{xy,\uparrow} + \tfrac{1}{6}d^\dagger_{e_g,\uparrow}d^\dagger_{xy,\uparrow}d^\dagger_{yz,\downarrow}\\ &+ \tfrac{1}{6}d^\dagger_{e_g,\uparrow}d^\dagger_{xy,\downarrow}d^\dagger_{yz,\uparrow} + \tfrac{1}{6}d^\dagger_{e_g,\downarrow}d^\dagger_{xy,\uparrow}d^\dagger_{yz,\uparrow} + \tfrac{1}{6}id^\dagger_{e_g,\uparrow}d^\dagger_{yz,\uparrow}d^\dagger_{zx,\downarrow} + \tfrac{1}{6}id^\dagger_{e_g,\uparrow}d^\dagger_{yz,\downarrow}d^\dagger_{zx,\uparrow}\\ &+ \tfrac{1}{6}id^\dagger_{e_g,\downarrow}d^\dagger_{yz,\uparrow}d^\dagger_{zx,\uparrow} + \tfrac{1}{2}d^\dagger_{e_g,\downarrow}d^\dagger_{xy,\downarrow}d^\dagger_{yz,\downarrow} - \tfrac{1}{2}id^\dagger_{e_g,\downarrow}d^\dagger_{yz,\downarrow}d^\dagger_{zx,\downarrow}.\end{aligned} \tag{B18}$$

4. $d^8 = t_{2g}^6 e_g^2$ configuration

After hopping, we can have a d^8 electron configuration as the intermediate state, with two electrons in the e_g orbitals and six electrons in the t_{2g} orbitals. Thus, we can denote d^8 as $t_{2g}^6 e_g^2$. There is only one possibility to arrange these electrons, giving rise to the orbital state

$$|L_z = 0\rangle = d^\dagger_{3z^2-r^2}d^\dagger_{x^2-y^2}|0\rangle. \tag{B19}$$

According to Hund's rule, the total spin momentum $\boldsymbol{S}$ has quantum number $S = 1$. The eigenstates of S_z are

$$\begin{aligned}|S_z = 1\rangle &= |\uparrow\uparrow\rangle,\\ |S_z = 0\rangle &= \frac{1}{\sqrt{2}}(|\uparrow\downarrow\rangle + |\downarrow\uparrow\rangle),\\ |S_z = -1\rangle &= |\downarrow\downarrow\rangle.\end{aligned} \tag{B20}$$

After the SOC, the total angular momentum $\boldsymbol{J}$ has quantum number $J = 1$, and the eigenstates are $|J_z = j_z\rangle = \varphi^\dagger_{j_z}|0\rangle$ ($j_z = 1, 0, -1$), with

$$\varphi^\dagger_1 = d^\dagger_{3z^2-r^2,\uparrow}d^\dagger_{x^2-y^2,\uparrow}, \tag{B21}$$

$$\varphi^\dagger_0 = \frac{1}{\sqrt{2}}(d^\dagger_{3z^2-r^2,\uparrow}d^\dagger_{x^2-y^2,\downarrow} + d^\dagger_{3z^2-r^2,\downarrow}d^\dagger_{x^2-y^2,\uparrow}), \tag{B22}$$

$$\varphi^\dagger_{-1} = d^\dagger_{3z^2-r^2,\downarrow}d^\dagger_{x^2-y^2,\downarrow}. \tag{B23}$$

5. $d^8 = t_{2g}^5 e_g^3$ configuration

After hopping, we can also have a d^8 electron configuration as the intermediate state, with three electrons in the e_g orbitals and five electrons in the t_{2g} orbitals. Thus, we can denote d^8 as $t_{2g}^5 e_g^3$. There are three possible states in which to arrange five electrons in the t_{2g} orbitals and two possible states for three electrons in the e_g orbitals. In the hole representation, we have

$$\begin{aligned}|k\rangle &= K^\dagger|0\rangle = d^\dagger_{e_g}d^\dagger_{xy}|0\rangle,\\ |p\rangle &= P^\dagger|0\rangle = d^\dagger_{e_g}d^\dagger_{yz}|0\rangle,\\ |r\rangle &= R^\dagger|0\rangle = d^\dagger_{e_g}d^\dagger_{zx}|0\rangle,\end{aligned} \tag{B24}$$

where e_g represents one of the e_g orbitals, either $3z^2 - r^2$ or $x^2 - y^2$. The projection of the physical orbital angular momentum $\boldsymbol{L}_{\text{physical}}$ onto the threefold orbital states gives an effective angular momentum $\boldsymbol{L} \cong -\boldsymbol{L}_{\text{physical}}$ with a quantum number $L = 1$. The eigenstates of L_z are similar to Eqs. (B11). According to Hund's rule, the total spin angular momentum $\boldsymbol{S}$ has quantum number $S = 1$ with eigenstates (B20). After the SOC, the total angular momentum $\boldsymbol{J}$ has quantum number $J = 0$, and the only eigenstate is

$$\begin{aligned}|J = 0\rangle = \varphi^\dagger_0|0\rangle &= \frac{1}{3}(|L_z = 1, wS_z = -1\rangle - |L_z = 0,\\ &\quad S_z = 0\rangle + |L_z = -1, S_z = 1\rangle)\\ &= \frac{1}{3\sqrt{2}}\big(d^\dagger_{e_g\downarrow}d^\dagger_{yz\downarrow} + id^\dagger_{e_g\downarrow}d^\dagger_{zx\downarrow} - d^\dagger_{e_g\downarrow}d^\dagger_{xy\uparrow}\\ &\quad - d^\dagger_{e_g\uparrow}d^\dagger_{xy\downarrow} + d^\dagger_{e_g\uparrow}d^\dagger_{yz\uparrow} - id^\dagger_{e_g\uparrow}d^\dagger_{zx\downarrow}\big)|0\rangle.\end{aligned} \tag{B25}$$

APPENDIX C: SINGLE-SITE HAMILTONIAN AND MAGNETIC MOMENTS

Given a system with a total angular momentum $\boldsymbol{J}$, the generic Hamiltonian should be a function of $\boldsymbol{J}$. Expanding the Hamiltonian in terms of polynomials of $\boldsymbol{J}$, we obtain

$$H_0 = \sum_\mu a_\mu J_\mu + \sum_{\mu\nu} b_{\mu\nu}J_\mu J_\nu + \sum_{\mu\nu\sigma} c_{\mu\nu\sigma}J_\mu J_\nu J_\sigma + \cdots. \tag{C1}$$

It is clear that H_0 is diagonal for different angular momentum quantum numbers J. For the cases considered in this paper, the largest J is 1. Thus, polynomials with more than two J_μ either are constant or can be absorbed into polynomials with lower order. We can truncate H_0 at the second order and obtain

$$H_0 = \sum_\mu a_\mu J_\mu + \sum_{\mu\nu} b_{\mu\nu}J_\mu J_\nu. \tag{C2}$$

For generic a_μ and $b_{\mu\nu}$, the eigenstates of H_0 are hard to obtain. Therefore, we focus on a simpler case, in which

$$H_0 = J_1\hat{\boldsymbol{e}}\cdot\boldsymbol{J} + J_2(\hat{\boldsymbol{e}}\cdot\boldsymbol{J})^2, \tag{C3}$$

where $\hat{\boldsymbol{e}} = (\sin\theta\cos\phi, \sin\theta\sin\phi, \cos\theta)$ is a unit vector. The eigenstates of H_0 are those of $\hat{\boldsymbol{e}}\cdot\boldsymbol{J}$. In the $J = 1/2$ subspace,

the eigenstates are

$$|\hat{\boldsymbol{e}}\cdot\boldsymbol{J}=1/2\rangle=\cos\frac{\theta}{2}\,|\Uparrow\rangle+e^{i\phi}\sin\frac{\theta}{2}\,|\Downarrow\rangle,\quad \text{with energy}\quad \frac{J_2+2J_1}{4},$$
$$|\hat{\boldsymbol{e}}\cdot\boldsymbol{J}=-1/2\rangle=\sin\frac{\theta}{2}\,|\Uparrow\rangle-e^{i\phi}\cos\frac{\theta}{2}\,|\Downarrow\rangle,\quad \text{with energy}\quad \frac{J_2-2J_1}{4}, \tag{C4}$$

where we have defined $|\Uparrow\rangle=|J_z=1/2\rangle$ and $|\Downarrow\rangle=|J_z=-1/2\rangle$. In the $J=1$ subspace, the eigenstates are

$$|\hat{\boldsymbol{e}}\cdot\boldsymbol{J}=1\rangle=\frac{1}{\sqrt{2}}[(\cos\theta\cos\phi-i\sin\phi)\,|x\rangle+(\cos\theta\sin\phi+i\cos\phi)\,|y\rangle-\sin\theta\,|z\rangle],\quad \text{with energy}\quad J_2+J_1,$$
$$|\hat{\boldsymbol{e}}\cdot\boldsymbol{J}=0\rangle=\sin\theta\cos\phi\,|x\rangle+\sin\theta\sin\phi\,|y\rangle+\cos\theta\,|z\rangle,\quad \text{with energy}\ \ 0,$$
$$|\hat{\boldsymbol{e}}\cdot\boldsymbol{J}=-1\rangle=\frac{1}{\sqrt{2}}[(\cos\theta\cos\phi+i\sin\phi)\,|x\rangle+(\cos\theta\sin\phi-i\cos\phi)\,|y\rangle-\sin\theta\,|z\rangle],\quad \text{with energy}\quad J_2-J_1. \tag{C5}$$

Without loss of generality, we assume $J_1>0$ and $J_2>0$. In this case the ground state of H_0 in the $J=1/2$ subspace is always $|\hat{\boldsymbol{e}}\cdot\boldsymbol{J}=-1/2\rangle$. In the $J=1$ subspace, the ground state is $|\hat{\boldsymbol{e}}\cdot\boldsymbol{J}=0\rangle$ if $J_2>J_1$ and is $|\hat{\boldsymbol{e}}\cdot\boldsymbol{J}=-1\rangle$ if $J_2<J_1$.

We are interested in the magnetic moments carried by these states. For a generic state in the $J=1/2$ space,

$$|\phi\rangle=a_\Uparrow\,|\Uparrow\rangle+a_\Downarrow\,|\Downarrow\rangle, \tag{C6}$$

one can calculate its magnetic dipole as

$$\begin{aligned}\langle\phi|J_x|\phi\rangle&=a_\Uparrow^*a_\Downarrow+a_\Downarrow^*a_\Uparrow,\\ \langle\phi|J_y|\phi\rangle&=-i(a_\Uparrow^*a_\Downarrow-a_\Downarrow^*a_\Uparrow),\\ \langle\phi|J_z|\phi\rangle&=a_\Uparrow^*a_\Uparrow-a_\Downarrow^*a_\Downarrow.\end{aligned} \tag{C7}$$

If we choose $|\phi\rangle$ to be the ground state $|\hat{\boldsymbol{e}}\cdot\boldsymbol{J}=-1/2\rangle$, then $\langle\boldsymbol{J}\rangle=-\hat{\boldsymbol{e}}$. Namely, the magnetic dipole is polarized along $-\hat{\boldsymbol{e}}$. For a generic state in the $J=1$ space,

$$|\psi\rangle=b_x\,|x\rangle+b_y\,|y\rangle+b_z\,|z\rangle, \tag{C8}$$

both the magnetic dipole and quadrupole appear. The magnetic dipole is

$$\langle\psi|\boldsymbol{J}|\psi\rangle=-i\boldsymbol{b}^*\times\boldsymbol{b}. \tag{C9}$$

We can see that the magnetic dipole vanishes for the unpolarized state $|\hat{\boldsymbol{e}}\cdot\boldsymbol{J}=0\rangle$ but equals $-\hat{\boldsymbol{e}}$ for the polarized state $|\hat{\boldsymbol{e}}\cdot\boldsymbol{J}=-1\rangle$. The magnetic quadrupole is defined as

$$Q_{\mu\nu}=\frac{1}{2}(J_\mu J_\nu+J_\nu J_\mu)-\frac{\boldsymbol{J}^2}{3}\delta_{\mu\nu}. \tag{C10}$$

Its expectation value for $|\psi\rangle$ can be obtained as

$$\langle\psi|Q_{\mu\nu}|\psi\rangle=\tfrac{1}{3}\delta_{\mu\nu}-\tfrac{1}{2}(b_\mu^*b_\nu+b_\nu^*b_\mu). \tag{C11}$$

Although the tensor $Q_{\mu\nu}$ has nine components, only five components are independent. They are

$$\begin{aligned}\langle\psi|Q_{3z^3-r^2}|\psi\rangle&=-\sqrt{3}(\langle\psi|Q_{xx}|\psi\rangle+\langle\psi|Q_{yy}|\psi\rangle)\\&=-\frac{b_x^*b_x+b_y^*b_y}{\sqrt{3}},\\ \langle\psi|Q_{x^2-y^2}|\psi\rangle&=\langle\psi|Q_{xx}|\psi\rangle-\langle\psi|Q_{yy}|\psi\rangle\\&=-(b_x^*b_x-b_y^*b_y),\\ \langle\psi|Q_{xy}|\psi\rangle&=-\frac{1}{2}(b_x^*b_y+b_y^*b_x),\\ \langle\psi|Q_{yz}|\psi\rangle&=-\frac{1}{2}(b_y^*b_z+b_z^*b_y),\\ \langle\psi|Q_{zx}|\psi\rangle&=-\frac{1}{2}(b_z^*b_x+b_x^*b_z).\end{aligned} \tag{C12}$$

APPENDIX D: FULL EQUATIONS FOR ELECTRIC POLARIZATION

Here we consider a generic J_1 and J_2 for the single-site Hamiltonian H_0, leading to a general expression for $\boldsymbol{b}$ with complex components. For the d^7 electron state, $\boldsymbol{a}=(\sin\theta/2,-e^{i\phi}\cos\theta/2)$ is considered to be a complex vector under the effective ordering field $\hat{\boldsymbol{e}}$. Then under this condition, the ground state has both dipole and quadrupole orders in the d^6 electron state and a dipole-only order d^7 electron state. The electric polarization $\boldsymbol{P}$ contains on-site contributions and mixed-site contributions. Due to a model-dependent anisotropic factor s_μ, we may define a scaled polarization $\tilde{P}_\mu=P_\mu/s_\mu$. The on-site contributions are given by

$$\begin{aligned}\tilde{P}^x_{\text{on}}=&(24|b_{1x}|^2+25|b_{1y}|^2)-(24|b_{2x}|^2+25|b_{2y}|^2)+3(\sqrt{3}-1)r_t(b_{1y}b_{1x}^*+b_{1x}b_{1y}^*-ib_{1z}b_{1x}^*+ib_{1x}b_{1z}^*+ib_{1z}b_{1y}^*-ib_{1y}b_{1z}^*\\&-b_{2y}b_{2x}^*-b_{2x}b_{2y}^*+ib_{2z}b_{2x}^*-ib_{2x}b_{2z}^*-ib_{2z}b_{2y}^*+ib_{2y}b_{2z}^*),\end{aligned} \tag{D1}$$

$$\tilde{P}^y_{\text{on}}=(b_{1x}^*b_{1y}+b_{1y}^*b_{1x})-(b_{2x}^*b_{2y}+b_{2y}^*b_{2x}), \tag{D2}$$

$$\tilde{P}^z_{\text{on}}=[-i(b_{1y}^*b_{1z}-b_{1y}b_{1z}^*)+i(b_{2y}^*b_{2z}-b_{2y}b_{2z}^*)]-8[(a_{1\Uparrow}^*a_{1\Downarrow}+a_{1\Downarrow}^*a_{1\Uparrow})-(a_{2\Uparrow}^*a_{2\Downarrow}+a_{2\Downarrow}^*a_{2\Uparrow})], \tag{D3}$$

where $r_t = \frac{t_0}{t_1}$, $s_x = 4C$, $s_y = 2C$, and $s_z = 10C$. We have defined a constant $C = et_1 I/(480\Delta)$, and I is the following integral:

$$I = \int \mathrm{d}^3 r\, d_{xy}(\boldsymbol{r}) x p_y(\boldsymbol{r}), \tag{D4}$$

which has cyclic permutation in x, y, and z. On-site contributions can be expressed in terms of the magnetic dipole and quadrupole,

$$\begin{aligned}
\tilde{P}^x_{\mathrm{on}} &= \left[\frac{49}{\sqrt{3}}\langle Q_{3z^2-r^2}\rangle_1 + \langle Q_{x^2-y^2}\rangle_1 - 3(\sqrt{3}-1)\big(2\langle Q_{xy}\rangle_1 + \langle J_x\rangle_1^{(d^6)} + \langle J_y\rangle_1^{(d^6)}\big)\right] \\
&\quad - \left[\frac{49}{\sqrt{3}}\langle Q_{3z^2-r^2}\rangle_2 + \langle Q_{x^2-y^2}\rangle_2 - 3(\sqrt{3}-1)\big(2\langle Q_{xy}\rangle_2 + \langle J_x\rangle_2^{(d^6)} + \langle J_y\rangle_2^{(d^6)}\big)\right], \\
\tilde{P}^y_{\mathrm{on}} &= -(\langle Q_{xy}\rangle_1 - \langle Q_{xy}\rangle_2), \\
\tilde{P}^z_{\mathrm{on}} &= \left[\langle J_x\rangle_1^{(d^6)} - 8\langle J_x\rangle_1^{(d^7)}\right] - \left[\langle J_x\rangle_2^{(d^6)} - 8\langle J_x\rangle_2^{(d^7)}\right].
\end{aligned} \tag{D5}$$

The mixed-site contributions are written as

$$\tilde{P}^x_{\mathrm{mix}} = 0, \tag{D6}$$

$$\begin{aligned}
\tilde{P}^y_{\mathrm{mix}} &= a_{1\Downarrow}a^*_{2\Downarrow}(b_{2y}b^*_{1x} - b_{2x}b^*_{1y} + 2ib_{2z}b^*_{1z}) + a_{2\Downarrow}a^*_{1\Downarrow}(b_{1x}b^*_{2y} - b_{1y}b^*_{2x} - 2ib_{1z}b^*_{2z}) \\
&\quad + a_{1\Downarrow}a^*_{2\Uparrow}(ib_{2z}b^*_{1x} + b_{2z}b^*_{1y} + ib_{2x}b^*_{1z} + b_{2y}b^*_{1z}) + a_{2\Uparrow}a^*_{1\Downarrow}(-ib_{1x}b^*_{2z} + b_{1y}b^*_{2z} - ib_{1z}b^*_{2x} + b_{1z}b^*_{2y}) \\
&\quad + a_{1\Uparrow}a^*_{2\Downarrow}(ib_{2z}b^*_{1x} - b_{2z}b^*_{1y} + ib_{2x}b^*_{1z} - b_{2y}b^*_{1z}) + a_{2\Downarrow}a^*_{1\Uparrow}(-ib_{1x}b^*_{2z} - b_{1y}b^*_{2z} - ib_{1z}b^*_{2x} - b_{1z}b^*_{2y}) \\
&\quad + a_{1\Uparrow}a^*_{2\Uparrow}(b_{2y}b^*_{1x} - b_{2x}b^*_{1y} - 2ib_{2z}b^*_{1z}) + a_{2\Uparrow}a^*_{1\Uparrow}(b_{1x}b^*_{2y} - b_{1y}b^*_{2x} + 2ib_{1z}b^*_{2z}),
\end{aligned} \tag{D7}$$

$$\begin{aligned}
\tilde{P}^z_{\mathrm{mix}} &= a_{1\Downarrow}a^*_{2\Downarrow}(-b_{2z}b^*_{1x} + ib_{2z}b^*_{1y} + b_{2x}b^*_{1z} + ib_{2y}b^*_{1z}) + a_{2\Downarrow}a^*_{1\Downarrow}(-b_{1x}b^*_{2z} - ib_{1y}b^*_{2z} + b_{1z}b^*_{2x} - ib_{1z}b^*_{2y}) \\
&\quad + a_{1\Downarrow}a^*_{2\Uparrow}(ib_{2x}b^*_{1y} - ib_{2y}b^*_{1x}) + a_{2\Uparrow}a^*_{1\Downarrow}(ib_{1x}b^*_{2y} - ib_{1y}b^*_{2x}) \\
&\quad + a_{1\Uparrow}a^*_{2\Downarrow}(ib_{2y}b^*_{1x} - ib_{2x}b^*_{1y}) + a_{2\Downarrow}a^*_{1\Uparrow}(ib_{1y}b^*_{2x} - ib_{1x}b^*_{2y}) \\
&\quad + a_{1\Uparrow}a^*_{2\Uparrow}(b_{2z}b^*_{1x} + ib_{2z}b^*_{1y} - b_{2x}b^*_{1z} + ib_{2y}b^*_{1z}) + a_{2\Uparrow}a^*_{1\Uparrow}(b_{1x}b^*_{2z} - ib_{1y}b^*_{2z} - b_{1z}b^*_{2x} - ib_{1z}b^*_{2y}).
\end{aligned} \tag{D8}$$

[1] S. Baroni, P. Giannozzi, and A. Testa, Green's-function approach to linear response in solids, Phys. Rev. Lett. **58**, 1861 (1987).

[2] R. D. King-Smith and D. Vanderbilt, Theory of polarization of crystalline solids, Phys. Rev. B **47**, 1651 (1993).

[3] R. Resta, Macroscopic electric polarization as a geometric quantum phase, Europhys. Lett. **22**, 133 (1993).

[4] R. Resta and D. Vanderbilt, Theory of polarization: A modern approach, in *Physics of Ferroelectrics: A Modern Perspective* (Springer, Berlin, 2007), pp. 31–68.

[5] N. A. Spaldin, A beginner's guide to the modern theory of polarization, J. Solid State Chem. **195**, 2 (2012).

[6] B. A. Bernevig and T. L. Hughes, *Topological Insulators and Topological Superconductors* (Princeton University Press, Princeton, NJ, 2013).

[7] D. Vanderbilt, *Berry Phases in Electronic Structure Theory: Electric Polarization, Orbital Magnetization and Topological Insulators* (Cambridge University Press, Cambridge, 2018).

[8] D. M. Nenno, C. A. C. Garcia, J. Gooth, C. Felser, and P. Narang, Axion physics in condensed-matter systems, Nat. Rev. Phys. **2**, 682 (2020).

[9] L. N. Bulaevskii, C. D. Batista, M. V. Mostovoy, and D. I. Khomskii, Electronic orbital currents and polarization in Mott insulators, Phys. Rev. B **78**, 024402 (2008).

[10] W. Eerenstein, N. D. Mathur, and J. F. Scott, Multiferroic and magnetoelectric materials, Nature (London) **442**, 759 (2006).

[11] C. Jia, S. Onoda, N. Nagaosa, and J. H. Han, Bond electronic polarization induced by spin, Phys. Rev. B **74**, 224444 (2006).

[12] H. Katsura, N. Nagaosa, and A. V. Balatsky, Spin current and magnetoelectric effect in noncollinear magnets, Phys. Rev. Lett. **95**, 057205 (2005).

[13] M. Mostovoy, Ferroelectricity in spiral magnets, Phys. Rev. Lett. **96**, 067601 (2006).

[14] H. Murakawa, Y. Onose, S. Miyahara, N. Furukawa, and Y. Tokura, Ferroelectricity induced by spin-dependent metal-ligand hybridization in $Ba_2CoGe_2O_7$, Phys. Rev. Lett. **105**, 137202 (2010).

[15] I. A. Sergienko and E. Dagotto, Role of the Dzyaloshinskii-Moriya interaction in multiferroic perovskites, Phys. Rev. B **73**, 094434 (2006).

[16] Y. Tokura, S. Seki, and N. Nagaosa, Multiferroics of spin origin, Rep. Prog. Phys. **77**, 076501 (2014).

[17] W. Windsch, A. J. Freeman, H. Schmid. Magnetoelectric interaction phenomena in crystals. Gordon and Breach Science Publishers London 1975. £ 10.90, Krist. Tech. **11**, K45 (1976).

[18] S.-W. Cheong and M. Mostovoy, Multiferroics: A magnetic twist for ferroelectricity, Nat. Mater. **6**, 13 (2007).

[19] K. T. Delaney, M. Mostovoy, and N. A. Spaldin, Super exchange-driven magnetoelectricity in magnetic vortices, Phys. Rev. Lett. **102**, 157203 (2009).

[20] M. Mostovoy, Multiferroics: Different routes to magnetoelectric coupling, npj Spintronics **2**, 18 (2024).

[21] M. Mostovoy, A. Scaramucci, N. A. Spaldin, and K. T. Delaney, Temperature-dependent magnetoelectric effect from first principles, Phys. Rev. Lett. **105**, 087202 (2010).

[22] M. Mostovoy, K. Nomura, and N. Nagaosa, Theory of electric polarization in multiorbital Mott insulators, Phys. Rev. Lett. **106**, 047204 (2011).

[23] J. B. Neaton, C. Ederer, U. V. Waghmare, N. A. Spaldin, and K. M. Rabe, First-principles study of spontaneous polarization in multiferroic $BiFeO_3$, Phys. Rev. B **71**, 014113 (2005).

[24] N. A. Spaldin and R. Ramesh, Advances in magnetoelectric multiferroics, Nat. Mater. **18**, 203 (2019).

[25] N. A. Spaldin and M. Fiebig, The renaissance of magnetoelectric multiferroics, Science **309**, 391 (2005).

[26] B. B. Van Aken, T. T. M. Palstra, A. Filippetti, and N. A. Spaldin, The origin of ferroelectricity in magnetoelectric $YMnO_3$, Nat. Mater. **3**, 164 (2004).

[27] G. Massarelli, B. Wu, and A. Paramekanti, Orbital Edelstein effect from density-wave order, Phys. Rev. B **100**, 075136 (2019).

[28] C.-K. Li, X.-P. Yao, and G. Chen, Writing and deleting skyrmions with electric fields in a multiferroic heterostructure, Phys. Rev. Res. **3**, L012026 (2021).

[29] S. Banerjee, S. Humeniuk, A. R. Bishop, A. Saxena, and A. V. Balatsky, Multipolar multiferroics in $4d^2/5d^2$ Mott insulators, Phys. Rev. B **111**, L201107 (2025).

[30] S.-S. Lee and P. A. Lee, U(1) gauge theory of the Hubbard model: Spin liquid states and possible application to κ-$(BEDT\text{-}TTF)_2Cu_2(CN)_3$, Phys. Rev. Lett. **95**, 036403 (2005).

[31] O. I. Motrunich, Orbital magnetic field effects in spin liquid with spinon Fermi sea: Possible application to κ-$(ET)_2Cu_2(CN)_3$, Phys. Rev. B **73**, 155115 (2006).

[32] O. I. Motrunich, Variational study of triangular lattice spin-1/2 model with ring exchanges and spin liquid state in κ-$(ET)_2Cu_2(CN)_3$, Phys. Rev. B **72**, 045105 (2005).

[33] P. Fazekas, *Lecture Notes on Electron Correlation and Magnetism* (World Scientific, Singapore, 1999).

[34] S. Maekawa, T. Tohyama, S. E. Barnes, S. Ishihara, W. Koshibae, and G. Khaliullin, *Physics of Transition Metal Oxides*, edited by M. Cardona, P. Fulde, K. Von Klitzing, R. Merlin, H.-J. Queisser, and H. Störmer, Springer Series in Solid-State Sciences, Vol. 144 (Springer, Berlin, 2004).

[35] G. Chen, Quadrupole moments and their interactions in the triangular antiferromagnet lattice FeI_2, Phys. Rev. Res. **5**, L032042 (2023).

[36] X. Bai, S.-S. Zhang, Z. Dun, H. Zhang, Q. Huang, H. Zhou, M. B. Stone, A. I. Kolesnikov, F. Ye, C. D. Batista, and M. Mourigal, Hybridized quadrupolar excitations in the spin-anisotropic frustrated magnet FeI_2, Nat. Phys. **17**, 467 (2021).

[37] W. Witczak-Krempa, G. Chen, Y. B. Kim, and L. Balents, Correlated quantum phenomena in the strong spin-orbit regime, Annu. Rev. Condens. Matter Phys. **5**, 57 (2014).

[38] A. S. Miñarro and G. Herranz, Emergent orbital dynamics in strongly spin-orbit coupled systems, arXiv:2505.16746.

[39] H. Kusunose, Description of multipole in f-electron systems, J. Phys. Soc. Jpn. **77**, 064710 (2008).

[40] Yu. F. Popov, A. M. Kadomtseva, G. P. Vorob'ev, V. A. Timofeeva, D. M. Ustinin, A. K. Zvezdin, and M. M. Tegeranchi, Magnetoelectric effect and toroidal ordering in $Ga_{2-x}Fe_xO_3$, J. Exp. Theor. Phys. **87**, 146 (1998).

[41] S. Voleti, D. D. Maharaj, B. D. Gaulin, G. Luke, and A. Paramekanti, Multipolar magnetism in d-orbital systems: Crystal field levels, octupolar order, and orbital loop currents, Phys. Rev. B **101**, 155118 (2020).

[42] K. Pradhan, A. Paramekanti, and T. Saha-Dasgupta, Multipolar magnetism in $5d^2$ vacancy-ordered halide double perovskites, Phys. Rev. B **109**, 184416 (2024).

[43] G. Chen, R. Pereira, and L. Balents, Exotic phases induced by strong spin-orbit coupling in ordered double perovskites, Phys. Rev. B **82**, 174440 (2010).

[44] G. Chen and L. Balents, Spin-orbit coupling in d^2 ordered double perovskites, Phys. Rev. B **84**, 094420 (2011).

[45] M. G. Yamada, M. Oshikawa, and G. Jackeli, Emergent SU(4) symmetry in α-$ZrCl_3$ and crystalline spin-orbital liquids, Phys. Rev. Lett. **121**, 097201 (2018).

[46] G. Cao and L. DeLong, *Frontiers of 4D- and 5D-Transition Metal Oxides* (World Scientific, Singapore, 2013).

[47] L. V. Pourovskii and S. Khmelevskyi, Hidden order and multipolar exchange striction in a correlated f-electron system, Proc. Natl. Acad. Sci. USA **118**, e2025317118 (2021).

[48] P. Santini, S. Carretta, G. Amoretti, R. Caciuffo, N. Magnani, and G. H. Lander, Multipolar interactions in f-electron systems: The paradigm of actinide dioxides, Rev. Mod. Phys. **81**, 807 (2009).

[49] Y. F. Popov, A. M. Kadomtseva, D. V. Belov, G. P. Vorob'ev, and A. K. Zvezdin, Magnetic-field-induced toroidal moment in the magnetoelectric Cr_2O_3, JETP Lett. **69**, 330 (1999).

[50] S. Hayami and H. Kusunose, Microscopic description of electric and magnetic toroidal multipoles in hybrid orbitals, J. Phys. Soc. Jpn. **87**, 033709 (2018).

[51] Y. Kuramoto, H. Kusunose, and A. Kiss, Multipole orders and fluctuations in strongly correlated electron systems, J. Phys. Soc. Jpn. **78**, 072001 (2009).

[52] S. Hayami, M. Yatsushiro, Y. Yanagi, and H. Kusunose, Classification of atomic-scale multipoles under crystallographic point groups and application to linear response tensors, Phys. Rev. B **98**, 165110 (2018).

[53] H. Kim *et al.*, Quantum spin nematic phase in a square-lattice iridate, Nature (London) **625**, 264 (2024).

[54] D. Hirai, H. Sagayama, S. Gao, H. Ohsumi, G. Chen, T.-H. Arima, and Z. Hiroi, Detection of multipolar orders in the spin-orbit-coupled $5d$ Mott insulator Ba_2MgReO_6, Phys. Rev. Res. **2**, 022063(R) (2020).

[55] Y. Zhou, H. Ye, J. Zhang, and S. Dong, Double-leaf Riemann surface topological converse magnetoelectricity, Phys. Rev. B **110**, 054424 (2024).

[56] G. Liu, M. Pi, L. Zhou, Z. Liu, X. Shen, X. Ye, S. Qin, X. Mi, X. Chen, L. Zhao, B. Zhou, J. Guo, X. Yu, Y. Chai, H. Weng, and Y. Long, Physical realization of topological Roman surface by spin-induced ferroelectric polarization in cubic lattice, Nat. Commun. **13**, 2373 (2022).